PREDICTING LOW-VELOCITY IMPACT DAMAGE IN COMPOSITE USING COHESIVE ELEMENT

Liu Hongquan1, Tan Shengang2
AVIC The First Aircraft Institute

Keywords: *Impact, delamination, matrix crack, FEA, interface elements, cohesive element*

Abstract

A numerical model is developed for predicting low-velocity impact induced force and damage in laminated composites. Stacked shell elements are employed to model the laminate plies with discrete interface elements being placed in pre-determined potential damage zones to model the initiation and propagation of in-plane matrix cracks and interlaminar delamination. These interface elements are governed by a bi-linear cohesive failure law. Cohesive element zones are determined by a separate FE analysis using a 3D solid element model to find the damage initiation sites. In order to save the computational effort, low-velocity impact is modelled by applying quasi-static indentation load. For a clustered cross-ply laminate, the model accurately calculated the impact load and damage area. It is shown that matrix cracks should be included in the model in order to simulate the delamination in adjacent interface. The practical outcome of this research is a validated FE modelling approach that can be further improved for predicting low-velocity impact damage.

1. Background

Current damage-tolerance design criteria for compression-loaded composite airframe structures are related to the impact energy or the depth of the dent in the structure caused by the impact event. The problem, related issues and solutions to low-velocity impacts that simulate dropped tools, runway debris and hail stones are well described in [1-3]. Testing of all candidate materials and configurations at structural levels is virtually impossible; therefore it is essential to develop reliable, efficient and robust predictive models that can be implemented into commercial finite element analysis packages to be used as a design tool.

Since the structural behaviour under impact is complex with matrix cracks and delaminations forming at different locations, many researchers have focused their attention on numerical modelling and simulation. For example, strength-based failure models have been employed for predicting damage initiation [4-7]. The well-known Chang-Chang model was developed for predicting in-plane fibre and matrix damage [4-5]. This approach has been improved by including the contribution of interlaminar shear and peel stresses [6]. Progress is also made by using much more detailed FE models and interface elements to calculate the local stresses after damage initiation to predict the damage progression [7]. Fracture mechanics methods have been employed for predicting delamination propagation [8-9]. Most commercial FE codes can perform calculations of the strain energy release rate. The method works well if pre-cracked structural models are realistic and with suitably shaped mesh. Adaptive mesh approach is recommended for irregular shaped delamination front. Although the energy based theories are physically more accurate, using the stress criteria to predict damage growth is also valid considering the very short duration of the contact event. Recently, cohesive zone models have been used to simulate both initiation and propagation under impact load [10-11]. Reviews of these methods can be found in [12-13]. This paper presents a finite element model

for predicting low-velocity impact damage in laminated composites.

2. Modelling approach

It is well recognised that a critical impact force (P_{cr}) exists that corresponds to the initiation of significant delamination damage [14-16]. Filtered impact force vs. time histories for five impact tests on quasi-isotropic laminate of 4 mm thickness at increased incident energy levels (5–30 J) are shown in Fig. 1a, indicating the critical impact force of about 5 kN. This measured force is very close to the predicted 4.8 kN using the following equation [15-16]:

$$P_{cr} = \sqrt{\frac{8\pi^2 E t^3 G_{IIC}}{9(1-\nu^2)}} \qquad (1)$$

where E is the laminate equivalent modulus, ν the Poisson's ratio and G_{IIC} the mode II toughness.

2.1 FE model

A rectangular test coupon is modelled using the commercial FE code Abaqus [17]. Laminate is modelled by continuum shell elements (SC8R). Damage initiation and propagation are modelled by stacking the shell elements with each element layer representing one lamina ply or several plies. To model delamination, cohesive interface elements (COH3D8) are placed between shell element layers as shown in Fig. 1a. To model the in-plan matrix cracking, cohesive elements are also placed within the lamina plane (Fig. 1b) along the line where in-plane stress transverse to the fibre direction (σ_{22}) is expected to be high enough to cause matrix cracking, i.e. the ply on the coupon's back-face, where impact-induced bending stress is the highest and in tension.

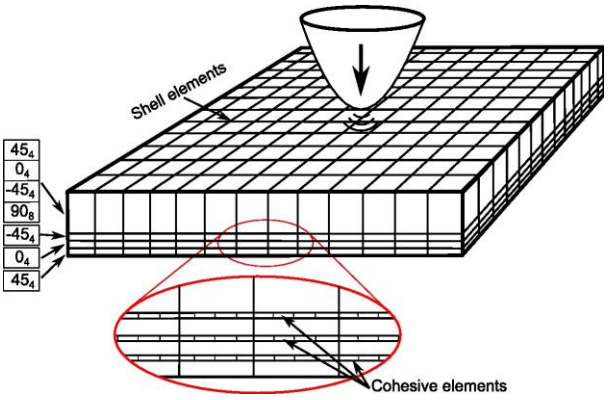

(a) multiple delaminations

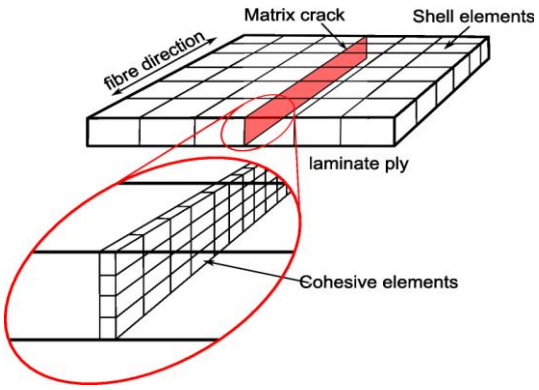

(b) matrix cracks

Fig. 1 Cohesive interface elements for modelling: (a) multiple delaminations near specimen's back face, and (b) in-plane matrix cracks in the back-face ply.

2.2 Cohesive law for the interface elements

Several cohesive models exist expressing the traction-separation relation of fracture interface. Some studies suggest that prediction is not sensitive to the cohesive law used as long as the fracture toughness (G_C) is the same [18-19]. In this research, a bilinear traction-separation law is used as shown in Fig. 2.

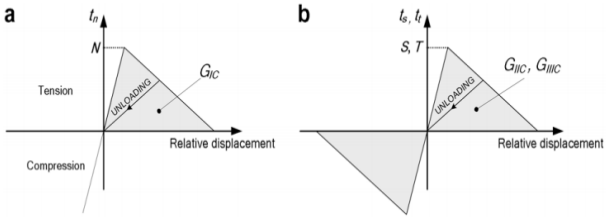

Fig. 2 Traction-separation law for: (a) mode I, and (b) model II and III delamination [10].

2.3 Modelling the influence of friction on delamination

Due to the Hertzian contact stress, high interlaminar shear stresses act on the upper interface close to the load point (calculated stresses are shown in Section 3). However, at this location only very small (negligible) delamination was found in experimental tests reported in the open literature. The high contact stress on the top interface can inhibit the shear-driving delamination. However, if the mode II cohesive law shown in Fig. 3(b) is used in the FE model, the influence of contact stress will not be taken into account; consequently predicted delamination area in the upper interface is much larger than test measured.

In this paper the influence of contact stress on shear dominant delamination is treated by adding the contribution of contact-induced friction (between adjacent plies) to the constitutive model of the interface element that is governed by a mode II cohesive law. A contact friction is introduced between two adjacent plies; the friction shear stress at the delamination crack wake will inhibit/reduce delamination growth.

The tension stiffness of the cohesive element is determined by the bilinear traction-separation law. However, under compressive load condition, the original normal stiffness still exists in order to stop penetration between adjacent plies. This normal stiffness is retained even after the total failure of the cohesive elements [10, 20]. In this research, a contact relationship was set up between the two plies, where a delamination exists, aiming at introducing friction between the plies. Under this circumstance, there are two spring bodies at the interface under compressive stress loading: one is the cohesive element and the other is a contact pair. The relation between cohesive elements and contact pair is illustrated in Fig. 4. Assume that the contact has a fixed stiffness equal to the compressive stiffness of the cohesive element, the cohesive stiffness does not degrade in compression after delamination, and the contact stress is equally distributed between the cohesive elements, then the indentation displacement can be calculated by:

$$\delta = \frac{P}{K_1 + K_2} \tag{2}$$

where K_1 and K_2 are the cohesive and contact stiffness, respectively, P the applied force.

The contact force (P_c) and friction force (P_f) are evaluated by:

$$P_c = K_2\delta = \frac{K_2}{K_1 + K_2}P \tag{3}$$

$$P_f = \mu P_c = \mu P\frac{K_2}{K_1 + K_2} \tag{4}$$

where μ is the coefficient of friction.

Eq. (4) shows the relation between μ and P_f. This value is selected within the range of experimentally measured friction coefficients in carbon fibre epoxy composites. Details are provided in Section 3.4 on the sensitivity study of this parameter. To implement the contact friction force into the ABAQUS code, a layer of cohesive elements of zero thickness is inserted between two adjacent laminate plies.

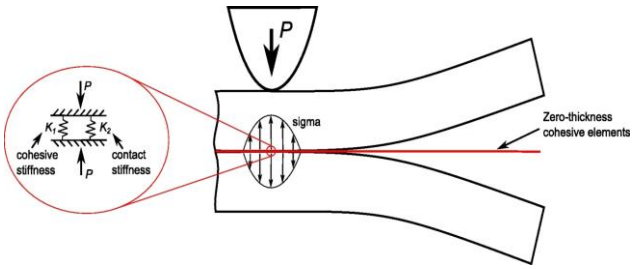

Fig. 3 Interface element and implementation into FEmodel

3. Results and Discussion

Test result in [10] is used to validate the proposed damage prediction model. The rectangular specimen had dimension of 65 mm × 87.5 mm with nominal thickness of 2 mm. The specimen was made of unidirectional Seal HS160/REM carbon/epoxy prepreg tapes (61.5% fibre content in weight). The stacking sequence that was modelled and reported in this paper is $[90_3/0_3]_s$. Specimen was simply supported by a steel plate with a rectangular cutout of 45 mm × 67.5 mm underneath the specimen. The hemisphere impactor diameter was 12.5 mm.

In [10] commercial FEA package Abaqus/Explicit solver was used, whereas in this paper Abaqus/Standard was employed for QSL simulation of the same test. Analysis was performed under the displacement-controlled loading condition, which is equivalent to the maximum displacement of low-velocity impact test at a given incident energy.

Only one quarter of the specimen was modelled due to the geometric symmetry. Continuum shell elements (SC8R) and cohesive elements (COH3D8) are employed to model the laminate and pre-defined interfaces, respectively. Since there is no interlaminar delamination between plies with same fibre orientation, cohesive interface elements were only inserted between the plies having different fibre orientations. For the stacking sequence $[90_3/0_6/90_3]$, two interfaces are modelled by cohesive elements, i.e. the upper interface 90/0 and lower interface 0/90. At the lower interface, where matrix cracking is more critical (due to large bending-induced stresses), a vertical interface of cohesive elements was inserted in order to model the matrix cracks, Fig. 4. This cohesive element layer was placed parallel to the local fibre orientation on the specimen symmetry plane.

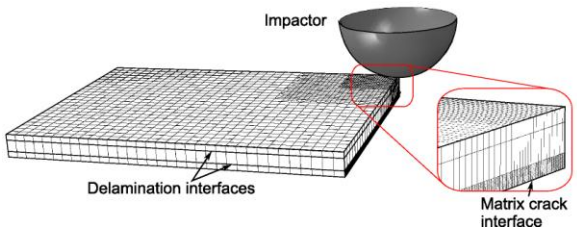

Fig. 4 FE model of a quarter of test specimen under quasi-static load

(Note the two interfaces in the cross-ply laminate $[90_3/0_6/90_3]$).

This model is similar to that used in [10]; except that QSL model and layered shell elements are used in this study in order to reduce computational effort (dynamic analysis and 3D brick elements were used in [10]). The smallest element size in the impact area is 0.25 × 0.25 mm and the cohesive element size is 0.05 mm. The impactor was modelled as a rigid body. This is reasonable due to the relatively smaller deformation of the impactor compared with the laminate. The size of the FE model is 45 mm × 67.5 mm, which is the same size as the rectangular cutout on the supporting frame. The four edges are modelled as simply supported boundary condition. Laminate elastic properties and cohesive model parameters used in the FE model are listed in Table 1. Symbols for the cohesive model can be found in Fig. 2.

Table 1 Laminate elastic properties and cohesive model parameters used in the analysis (from [10]).

Laminate	Cohesive model (Fig. 3)
E_{11} = 93.7 GPa; E_{22} = E_{33} = 7.45 GPa	K_N = 120 GPa/mm; K_S = K_T = 43 GPa/mm (Stiffness)
G_{12} = G_{23} = G_{13} = 3.97 GPa	N = 30 MPa; S = T = 80 MPa (Critical stress)
ν_{12} = ν_{23} = ν_{12} = 0.261	G_{IC} = 520 J/m^2; G_{IIC} = G_{IIIC} = 970 J/m^2

3.1 Undamaged plate under QSL

First, FE analysis of residual stresses due to elevated temperature curing process was performed. Residual transverse shear stresses are found to exist only at the specimen's free boundaries; this should not affect the impact behaviour at the specimen centre. However, residual in-plane stresses transverse to fibre orientation are uniformly distributed with average values of 30-35 MPa, which is about 50% of the tensile strength of resin matrix. Due to these initial stresses, matrix cracking will occur at early stage of impact, which acts as the initiation mechanism for interlaminar delamination at the ply interface. This was also reported in [21].

QSL analysis was subsequently performed simulating an impact test reported in [10]. For the stress analysis of undamaged specimen, solid elements are used with one element per ply. For impact energy of 1.5 J, maximum displacement at the specimen centre due to the impact was measured as 1.88 mm. This displacement is applied to the QSL model resulting in a reaction force of 1640 N. Fig. 5 shows the stress distribution at three interfaces: the first interface between the top two plies (90/90), the "upper interface" (90/0) and "lower interface" (0/90). In the latter two cases, the ply orientations are different at the interface and hence the transverse stresses are expected to be much higher due to the stiffness mismatch.

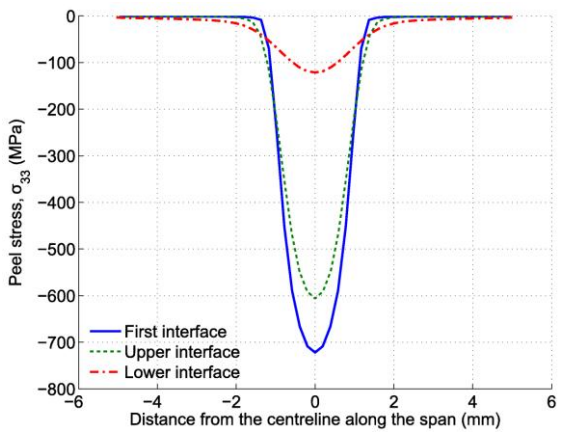

(a) Peel stresses

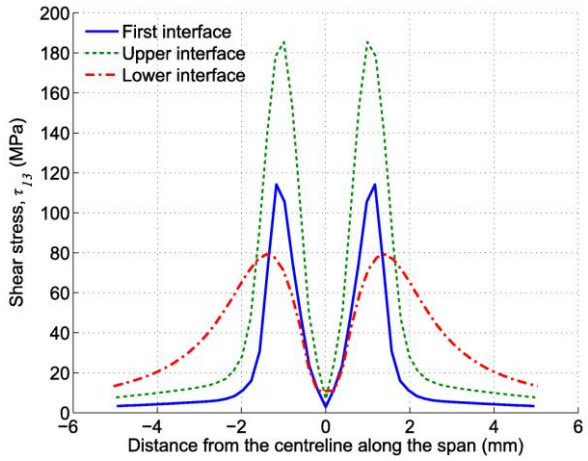

(b) Shear stresses

Fig. 5 Interlaminar stress distribution along the plate span in three interfaces of cross-ply $[90_3/0_6/90_3]$.

High transverse compressive (contact) stress (σ_{33}) acts at the first (90/90) and upper interface (90/0), Fig. 6a. Interlaminar shear stress (σ_{13}) is the highest (180 MPa) at the upper interface, Fig. 6b. However, little delamination damage was found in the test in [10]. Many published research also supports this evidence that apart from an indentation the top interface suffers virtually no delamination damage. This damage suppression mechanism is due to the higher compressive stress (σ_{33}) in the same location. The modelling method to account for this effect on delamination suppression is described in Section 2.3.

The lower interface (0/90) also suffers high shear stress and it spreads in a larger region compared to that on the upper interface, Fig. 6(b). At this stress level (80 MPa) it is possible to initiate delamination in the lower interface. However, the main mechanism for lower interface delamination is found to be the matrix cracking on the last ply (90_3). To demonstrate this, distribution of the in-plane transverse stress is plotted in Fig. 7. It shows stress component σ_{22} in the local fibre coordinate, or σ_y in the coordinate in Fig. 7). The maximum stress at the back face under the applied displacement 1.88 mm (equivalent to 1.5 J impact energy) is about 100 MPa at the lower interface (0/90), which exceeds the matrix tensile strength of about 60-70 MPa. Adding the curing process induced residual stress, which is about 30-35 MPa in the resin matrix transverse to the local fibre direction (details can be found in [22]), the total σ_{22} stress is even higher. Therefore, it is the σ_{22} stress component that induced matrix cracking first, which lead to delamination at the adjacent interface (0/90).

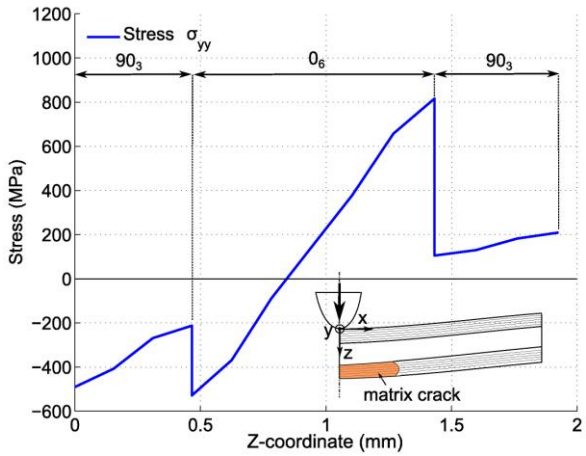

Fig. 6 In-plane transverse stress ($\sigma_{22} = \sigma_y$) distribution through the thickness of cross-ply $[90_3/0_6/90_3]$. Note: σ_{22} at the lower interface (0/90) is about 100 MPa.

3.2 Predicted damage and interlaminar stresses

In the subsequent analyses, both matrix cracking and delamination were modelled by cohesive failure model under displacement-controlled QSL equivalent to impact energy 1.5 J. The model takes into account the friction action at the upper interface where there is much higher compressive load. The coefficient of friction μ = 0.9 is used. A sensitivity study of this parameter is presented in Section 3.4. Interface elements for modelling matrix cracks were introduced

along the middle line of the last stack of three 90° plies (Fig. 4). This was guided by the maximum bending deformation in this location. Predicted delamination area and comparison with a reference model and experimental measurement in [10] is shown in Fig. 7. Reasonably good agreement is achieved. Measured delamination at the upper interface was not available for this layup $[90_3/0_3]_s$, but for the specimen of stacking sequence $[0_3/90_3]_s$, which has the same geometry and same bending stiffness to the layup $[90_3/0_3]_s$, negligible delamination area was found in the test on the upper interface [10, 20].

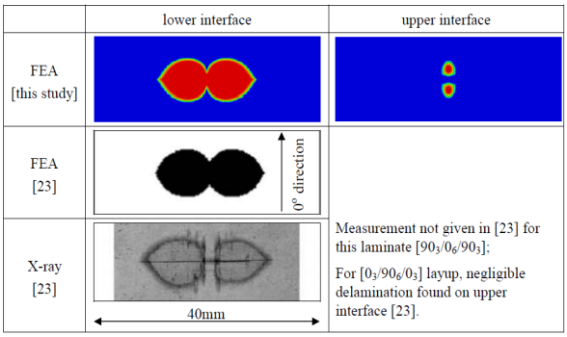

Fig. 7 Predicted delamination area and experimental measurement (impact energy 1.5 J)

Computed interlaminar peel and transverse shear stresses at the upper interface are plotted in Fig. 8 with and without modelling the matrix crack at the back face. Delamination initiation and propagation is also modelled using the aforementioned cohesive failure model. Predicted delamination length at the upper interface is about 2.5 mm (Fig. 8b). Following observations can be made. First, presence of matrix crack in the specimen back face has little influence on the calculated interlaminar peel and shear stresses on the upper interface. Second, interlaminar shear stress is the highest at the two tips of the delamination crack (Fig. 8b). However, the high compressive peel stress (Fig. 8a) has inhibited the propagation of delamination; consequently, despite the high shear stresses at the delamination tips, predicted damage length on the upper interface is very small as shown in Fig. 8, which agrees well with experimental observation and measurement in [20] for a similar layup $[0_3/90_6/0_3]$.

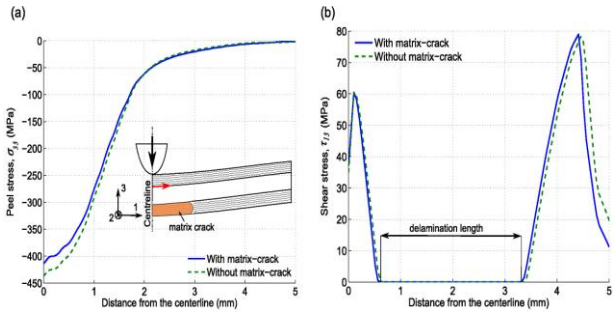

Fig. 8 Computed peel (a) and shear stress (b) at the upper interface (90/0) with and without modelling matrix crack at the back face.

Peel stress distribution at the lower interface is plotted in Fig. 9 with and without modelling the matrix crack in the back face. Before the matrix crack happens, very small positive peel stress exists in the lower interface along the matrix crack direction (Fig. 5a). After the matrix cracking happens, high positive peel stress is found in the lower interface, which will promote the mode I delamination. This observation was also reported by Chang [21].

Delamination at the lower interface is triggered by the matrix crack. This phenomenon onsets and propagates delamination in mode I (since the shear stress is zero on the symmetry plane). After this event, the interlaminar delamination also propagates perpendicular to the matrix-crack plane, making the delamination shape wider as shown by the images in Fig. 7. In order to understand which stress component drives the delamination growth in the transverse-to-matrix-crack direction, interlaminar shear stress on the lower interface is plotted along the matrix crack direction as shown in Fig. 10. The delamination crack length at its centreline is about 7 mm. The crack propagation is driven by the mode II, because the peel stress is almost zero and shear stress reaches peak value of 80 MPa at the crack tip. Given that the average strength of transverse shear for carbon/epoxy composite is 70-100 MPa, this stress level can cause delamination propagation in the transverse direction (σ_{23} is plotted in the figure).

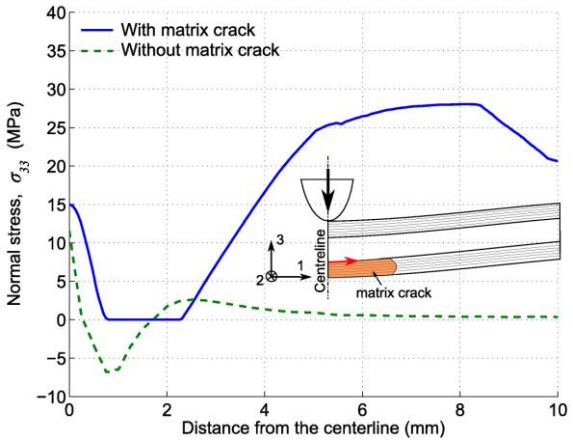

Fig. 9 Peel stress distribution in the lower interface (0/90) along the matrix crack direction.

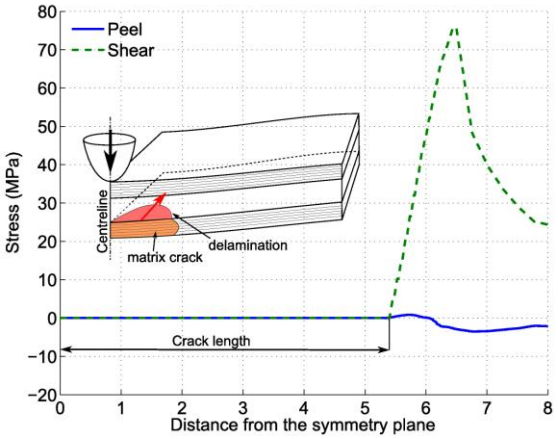

Fig. 10 Lower interface shear stress distribution along the plate span in local fibre orientation.

3.3 Influence of matrix cracking on predicted delamination area

Comparison of predicted delamination shape and area (with and without allowing matrix cracking in the models) with experimental measured delamination is shown in Fig 11. Without modelling the matrix cracking effect, predicted delamination area is significantly smaller and also in wrong shape. Measured delamination long-axis is oriented in the fibre direction of the lower ply, where in-plane matrix crack happened and modelled. The matrix crack therefore triggers the delamination and strongly affects the direction of the delamination crack propagation (resulting in the characteristic peanut shape). In the stacked cross-ply case, allowing a single matrix crack to form and develop at the centre of the back ply has improved the model accuracy resulting in a realistic delamination shape and size.

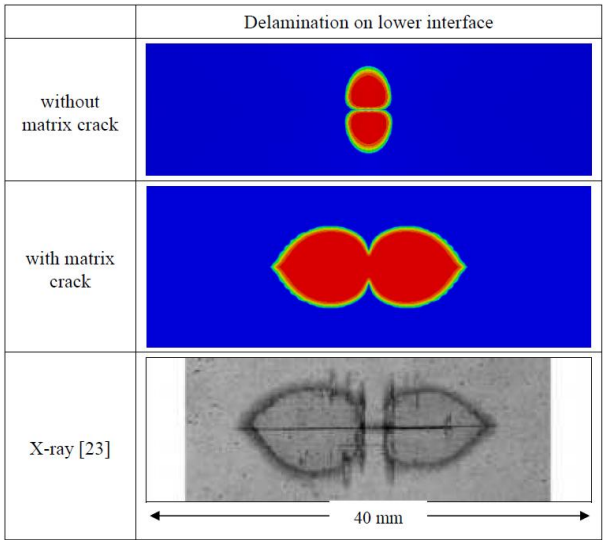

Fig. 11 Predicted delamination on lower interface with and without allowing matrix cracking.

4. Conclusions

A numerical model has been developed for predicting low-velocity impact damage in laminated composites. To improve the computational efficiency, following features are implemented into the model: a) quasi-static load is applied to simulate low-velocity impact; b) laminate plies are modelled by stacked thick shell elements; each shell element layer represents a group of plies of the same fibre orientation; c) interface elements are placed in zones of potential in-plane matrix cracks and interlaminar delamination; d) contact force-induced friction stress that inhibits delamination in the upper interface is modelled by a novel interface element.

Based on the numerical simulation of a stacked cross-ply laminate $[90_3/0_6/90_3]$, following conclusions can be drawn.

- Quasi-static load model can simulate low-velocity impact induced force and damage.

- Matrix cracking plays an important role in initiating delamination in adjacent interface. The most critical matrix crack for thin laminates is on the specimen's back face. Modelling matrix crack has enabled prediction of realistic delamination shape and area.
- After delamination initiation, high positive peel stress develops on the lower interface along the matrix crack direction, which promotes further delamination in mode I. Consequently the delamination crack propagates along the lower-ply matrix crack direction. This peel stress driving delamination can explain the peanut-shaped delamination with the longer axis being the fibre direction of the adjacent lower ply.
- Delamination also propagates in the direction transverse to the matrix crack direction. This is mainly driven by the transverse shear stress acting on the delamination front.
- On the upper interface, where high shear stresses act, mode II delamination propagation is inhibited by the contact force-induced friction stress.

References

[1] Davies GAO, Olsson R. Impact on composite structures. The Aeronautical Journal 2004; 108: 541-563

[2] Abrate S. Impact on Composite Structures. Cambridge University Press, 1998.

[3] Abrate S. Impact on laminated composites: recent advances. Applied Mechanics Reviews 1994; 47(11): 517–44.

[4] Chang F-K, Chang K-Y. A progressive damage model for laminated composites containing stress concentrations. J Composite Mater. 1987, 21:834-855.

[5] Choi HY, Chang FK. A model for predicting damage in graphite/epoxy laminated composites resulting from low-velocity point impact. J Compos Mater 1992; 26:2134-69.

[6] Hou JP, Petrinic N, Ruiz C. A delamination criterion for laminated composites under low-velocity impact. Compos Sci Technol 2001; 61:2069-74.

[7] Bouvet C, Castanie B, Bizeul M, Barrau, J-J. Low velocity impact modelling in laminate composite panels with discrete interface elements. Int J of Solids and Structures 2009; 46:2809-2821.

[8] Zheng S, Sun CT. A double-plate finite-element model for the impact-induced delamination problem. Compos Sci Technol 1995; 53(1):111-8.

[9] Li CF, Hu N, Yin YJ, Sekine H. Low-velocity impact-induced damage of continuous fibre-reinforced composite laminates part 1. An FEM numerical model. Compos Part A – Appl Sci. 2002; 33:1055-62.

[10] Aymerich F, Dore F, Priolo P. Simulation of multiple delaminations in impacted cross-ply laminates using a finite element model based on cohesive interface elements. Compos Sci Technol 2009; 69:1699-1709.

[11] Borg R, Nilsson L, Simonsson K. Simulation of low velocity impact on fibre laminates using a cohesive zone delamination model. Compos Sci Technol 2004; 64:279-88.

[12] Elder DJ, Thomson RS, Nguyen MQ, Scott ML. Review of delamination predictive methods for low speed impact of composite laminates, Compos Struct 2004; 66:677-83.

[13] Wisnom MR. Modelling discrete failures in composites with interface elements 2010; Composites Part A 2010; 41: 795-805.

[14] Sjoblom P, Hwang B. Compression-after-impact: the $5,000 data point. Proc 34th Int SAMPE Symposium, Reno, Nevada, May 8-11, 1989, pp. 1411-1421.

[15] Davies GAO, Robinson P. Predicting failure by debonding/delamination. In: Debonding/Delamination of Composites. AGARD-CP-530, Neuilly sur Seine: AGARD, 1992. p. 5.1-5.28

[16] Davies GAO, Zhang X. Impact damage prediction in carbon composite structures, Int J Impact Engng 1995; 16: 149-170.

[17] ABAQUS User's Guide, Version 6.10, Published by Simulia.

[18] Shet C, Chandra N. Analysis of energy balance when using cohesive zone models to simulate fracture process. Eng Mater Tachnol 2002; 124: 440-50.

[19] Willamis JG, Hadavinia H. Analytical solutions for cohesive zone models. Mech Phys Solids 2002; 50(4): 809-25.

[20] Aymerich F, Dore F, Priolo P. Prediction of impact-induced delamination in cross-ply composite laminates using cohesive interface elements. Compos Sci Technol 2008; 68:2383-90.

[21] Chang F.K, Choi H.Y, Jeng S.T. Study on impact damage in laminated composites. Mechanics of Materials 1990; 10: 83-95.

[22] Liu H. Ply clustering effect on composite laminates under low-velocity impact using FEA, MSc Thesis, Cranfield University, 2012.

[23] Schön J. Coefficient of friction of composite delamination surfaces. Wear 2000; 237:77–89.

[24] Ghelli D, Minak G. Low velocity impact and compression after impact tests on thin carbon/epoxy laminates, Composites: Part B 2011; 42: 2067–79.

Contact Author Email Address

For further contact:
Emai 1: xiaoliu810609@sina.com
Emai 2: 31994245@qq.com

Copyright Statement